

Interferometric methods for spatio temporal seismic monitoring in underground mines

Philippe Dales,¹ Pascal Audet,¹ Gerrit Olivier² and Jean-Philippe Mercier³

¹Department of Earth and Environmental Sciences, University of Ottawa, Ottawa, ON K1N 6N5, Canada. E-mail: pdales@gmail.com

²Institute of Mine Seismology, Hobart, Tasmania

³Oyu Tolgoi Mine, Khanbogd, Mongolia

Accepted 2017 May 29. Received 2017 March 31; in original form 2016 October 21

SUMMARY

In active underground mining environments, monitoring of the rockmass has important implications for both safety and productivity. Monitoring can be accomplished by exploiting the many passive seismic sources (microearthquakes, drilling, ore-crushers etc.) around the mine on the condition they can be accurately detected and located. We implement a popular beamforming-like approach that uses cross-correlation functions in a maximum likelihood search to locate sources of seismic energy. We illustrate the technique with a synthetic example in which two simultaneous sources are located and discuss briefly the effects of different processing parameters. We demonstrate the effectiveness of this technique by monitoring both impulsive sources (microearthquakes) and other persistent sources (drilling and ore-crushers) in two active underground mines. We then propose how this information can be used in conjunction with ambient seismic noise interferometry to estimate seismic Green's functions under temporally variable and anisotropic wavefield conditions. Alternatively, we demonstrate how stable persistent sources, typically seen as contaminants in ambient noise applications, can be used to monitor changing rockmass conditions and potentially guide mining operations.

Key words: Seismic interferometry; Seismic monitoring; Wave propagation; Body waves.

1 INTRODUCTION

Automated detection and location of seismic sources is a fundamental problem in seismology, with practical applications for monitoring and earthquake early warning (e.g. Allen & Kanamori 2003). Traditionally, due to the impulsive nature of earthquake rupture, detection has been accomplished using some type of triggering scheme (e.g. Allen 1978) while location has involved inverting P- and S-phase arrival times picked at multiple sensors (Geiger 1912). Although effective at detecting single impulsive sources, phase-picking methods perform poorly when sources are weak relative to background noise, or during periods containing multiple sources, and fail completely in detecting and locating persistent sources where onset times cannot be identified.

In the case of weak or persistent sources, cross-correlation techniques allow for the measurement of time difference of arrivals (or time-delays) between pairs of stations. The time-delays are estimated by picking the lag-time of the maximum peak in the cross-correlated waveforms (Knapp & Carter 1976). The delay-time for each station pair corresponds to a hyperbolic curve in 2-D (or a paraboloid in 3-D) along which the source is likely to lie. These curves are then computed for multiple station pairs with their optimal intersection point giving the best estimate of source location (Marchand 1964). In seismology, this method has been used for example to locate both non-volcanic tremor within slow earthquakes

(Obara 2002) and the primary origin of the 26 s microseism noise from ambient noise correlations (Shapiro *et al.* 2006). The primary drawback to this method is that using only a single peak value in the cross-correlation function (CCF) leads to failure under strongly scattering conditions or time periods when multiple sources are active. One method found to increase the robustness of the time-delay locator under noisy and reverberant conditions is by equally weighting all frequencies of the CCFs (Knapp & Carter 1976).

Under conditions where it is difficult (or incorrect in the multi source case) to pick single arrival times from the original waveforms, or single time-delays from the cross-correlated waveforms, beamforming techniques offer a robust solution. Instead of inverting for specific arrival times, beamforming involves phase-delaying and stacking waveforms for each possible source location based on traveltimes calculated from that location to each station. This is effectively a grid search where the point with the highest stacked amplitude represents the most probable source location. Optimality and variations of this procedure were originally proposed by Hahn & Tretter (1973) and then extended to the multiple source case by Wax & Kailath (1983).

It should be noted that beamforming techniques can also be thought of as part of a more general framework called matched-field processing (MFP), originally introduced by Bucker (1976) for passive target localization (e.g. submarines) in underwater acoustics. MFP involves the systematic comparison of data recorded on

a sensor array with synthetic data generated by a wave-propagation model. At each potential location, the forward model is compared to the real data, resulting in a probability map of potential source locations. This comparison is most commonly done using the Bartlett processor which correlates the real and synthetic data (Kuperman & Turek 1997). In this framework, beamforming can be thought of as the special case where the synthetic signals are appropriately shifted delta functions. Some examples of direct applications of MFP in seismology include locating bubble collapse events to map hydrothermal systems (e.g. Cros *et al.* 2011) and locating microearthquakes buried in anthropogenic noise associated with hydrocarbon extraction (e.g. Corciulo *et al.* 2012).

Beamforming can be accomplished either using the original or cross-correlated waveforms by simply changing how the delay-times (required for signal shifting) are calculated. Using the original waveforms, the appropriate delay-times are the direct traveltimes between each station and the potential source location (see e.g. the source scanning algorithm by Kao & Shan (2004) to locate non-volcanic tremor events in Northern Cascadia). When beamforming using cross-correlated waveforms, the delay-times are instead calculated as the difference in traveltimes from the source location to each station in the pair. This method of time-delay beamforming appears to have been discovered independently many times and is also referred to as beamforming along diffraction hyperbolas (Wassermann 1997), steered response power with phase-transform (SRP-PHAT) (DiBiase 2000; DiBiase *et al.* 2001), the source scanning algorithm (Ballmer *et al.* 2013; Droznić *et al.* 2015) (same name but different method than Kao & Shan (2004)) and cross-correlation beamforming (Ruirok *et al.* 2017). As with the time-delay locator, the cross-correlations are often spectrally whitened prior to localization to decrease the sensitivity of the method to environmental conditions (DiBiase *et al.* 2001). This method of beamforming using spectrally whitened cross-correlations is robust, intuitive and easy to implement. To simplify the terminology (and hopefully appeal to the ambient noise community) we refer to this technique as an interferometric locator or InterLoc for short.

While we refer to interferometric methods as techniques involving the interference of waveforms through cross-correlation, the term ‘seismic interferometry’ typically refers to the cross-correlation and summation of seismograms to create virtual events, a technique pioneered by Claerbout (1968). It has since been demonstrated that cross-correlations of ambient seismic noise can be used to construct estimates of the Green’s function between sensor pairs, effectively turning each sensor into a virtual source (Roux & Kuperman 2004; Shapiro & Campillo 2004; Sabra *et al.* 2005; Campillo 2006). Since sensor positions are generally fixed, ambient noise interferometry allows for very sensitive monitoring of temporal velocity changes in the medium between the sensor pair (Sens-Schönfelder & Wegler 2006; Brenguier *et al.* 2008). One of the primary limitations of this method is the reliance on either a fully diffuse wavefield (i.e. equipartition of modes) or a homogeneous distribution of spectrally white noise sources (Lobkis & Weaver 2001; Weaver & Lobkis 2004), although these conditions can be relaxed slightly in the presence of scatterers which act as secondary sources (Snieder 2004). In active underground mines, where few strong sources produce anisotropic and directional wavefields, conditions are generally not suitable to estimate seismic Green’s functions (Olivier *et al.* 2015). It is possible, however, to isolate periods where conditions are suitable by exploiting the temporal and spatial variability in the wavefield. In this case, an effective technique to monitor the seismic wavefield becomes essential.

In this paper we describe the interferometric locator and show its potential for spatio temporal monitoring in underground mines. To illustrate the technique we use a synthetic example in which two sources are generated simultaneously. Next, we present the challenges and propose solutions to effectively detect and locate different types of seismic sources. Following from this, we use data recorded at two active underground mines to demonstrate the robustness of this technique by monitoring both impulsive (microearthquakes) and persistent sources (drilling and ore-crushers). We then propose integrating seismic monitoring with ambient noise interferometry to improve estimates of seismic Green’s functions under temporally variable and anisotropic wavefield conditions. Lastly, we demonstrate the potential of using stable persistent sources to monitor changing rockmass conditions and guide mining operations.

2 THE INTERFEROMETRIC LOCATOR

Mathematical expression of the InterLoc method begins with the cross-correlation $C_{12}(t)$ of two signals, $u_1(t)$ and $u_2(t)$, recorded at separate sensors and expressed in the frequency domain as

$$C_{12}(t) = \mathcal{F}^{-1}[\Psi_{12}(\omega)U_1(\omega)U_2^*(\omega)], \quad (1)$$

where \mathcal{F}^{-1} is the inverse Fourier transform, $U_1(\omega)$ and $U_2(\omega)$ are the Fourier transforms of $u_1(t)$ and $u_2(t)$, ω is angular frequency, and $\Psi(\omega)$ is the spectral weighting (whitening) coefficient,

$$\Psi_{12}(\omega) = \frac{1}{|U_1(\omega)U_2^*(\omega)|}. \quad (2)$$

Then to evaluate the likelihood P of a seismic source being located at point $\vec{q} = (x, y, z)$ we compute all cross-correlations for N sensor pairs, delay them with respect to \vec{q} and sum the zero lag samples according to

$$P(\vec{q}) = \sum_{i=1}^N \sum_{j=i+1}^N C_{ij}(\tau_i - \tau_j), \quad (3)$$

where N is number of sensors and τ_n is the traveltime from location \vec{q} to sensor n . We refer to the function P normalized by total number cross-correlations (N choose 2 for unique sensor pair combinations) as the output power, while P evaluated at some point \vec{q} in space is referred to as a functional evaluation (FE) for that given point. By computing FEs at every point in space, the most likely source location \vec{q}_s is then given where the output power is maximum

$$\vec{q}_s = \underset{\vec{q}}{\operatorname{argmax}} P(\vec{q}). \quad (4)$$

3 SYNTHETIC EXAMPLE

To illustrate the location technique we use synthetic data generated with the Salvus spectral element wave propagation package (Afanasiev *et al.* 2017). The simulation setup (Fig. 2, left panel) consists of a 100×100 m (0.3 m grid spacing) 2-D scalar medium in which displacement is recorded at 16 pseudo-randomly located sensors. This geometry attempts to emulate the non-uniform spatial distribution of sensors typical of seismic systems in underground mines. The two synthetic sources have source-time functions corresponding to a microearthquake and ore-crusher respectively (Fig. 1) and have been normalized to have equal energy. An example of the resulting synthetic recordings (spectrally whitened) at two sensors, as well as their cross-correlation, are shown in the left panel of

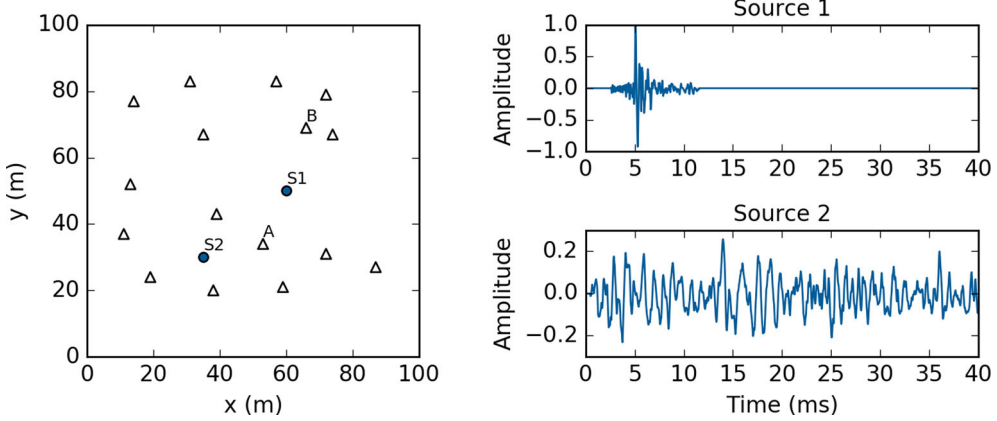


Figure 1. Left: geometry of sensors (triangles) and sources (circles) used in the wave propagation simulation. Right: the source-time functions for the two sources which are modelled after a microearthquake (source 1) and an active ore-crusher (source 2) respectively.

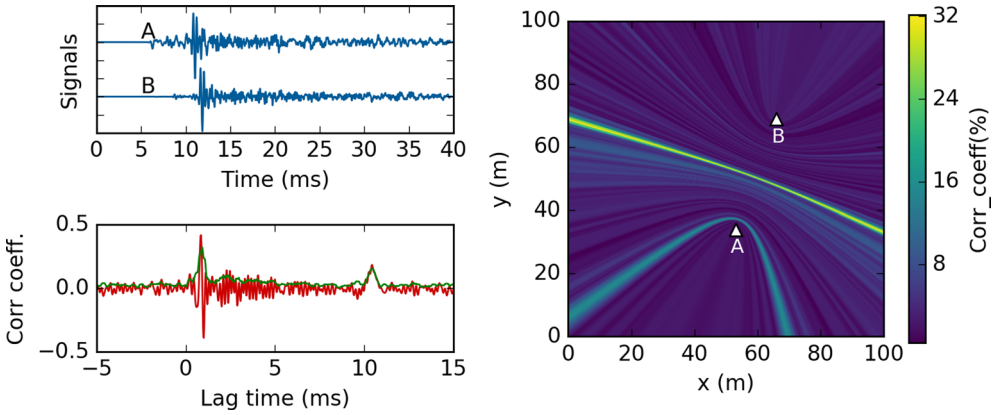


Figure 2. Left: example of the synthetic recordings at sensors A and B (top) and the resulting cross-correlation of the two waveforms (bottom). Green solid line in bottom plot is the smoothed signal used in computing the output power. Right: mapping of the cross-correlation into 2-D space assuming a constant velocity model. Each lag time in the CCF corresponds to a parabola in space along which the correlation value is directly mapped. At any point along a parabola the difference in traveltime (distance) to each sensor remains constant.

Fig. 2. Note how each peak in the cross-correlated waveform corresponds to a unique source. Before computing the output power the CCFs are smoothed using a sliding window root-mean-square with a window length of 0.2 ms (see Section 4.2).

The right panel of Fig. 2 demonstrates how this single CCF is mapped out into space. With a constant velocity model (i.e. straight propagation paths or rays), each lag time in the cross-correlation maps out to a parabola in 2-D space along which the time difference of arrival remains constant. Therefore, a peak in correlation at a given lag-time indicates that a source is likely to lie somewhere along the parabola associated with that lag time. With one pair this provides minimal constraint on location, but after computing and summing the output power for many sensor pairs the true source locations are naturally revealed (Fig. 3). In the summing process, the non-spurious correlations in each CCF stack constructively, while the spurious correlations, which are not spatially coherent between CCFs, do not.

In this example, the only free parameter is the velocity of the medium, known to be 3000 m s^{-1} ; however the method remains robust even under poorly estimated velocity models. Estimating and improving the velocity model can be accomplished using the InterLoc method itself as the correct velocity will produce the most focused maximum likelihood volumes. In a constant velocity medium, the optimal value can be obtained by iteratively adjusting the velocity model and recalculating the output power until the global maximum is found, as demonstrated in Fig. 4.

4 PRACTICAL IMPLEMENTATION AND CONSIDERATIONS

Similar to ambient noise interferometry, this location method entails computing a set of CCFs semi-continuously in time within finite length windows. Depending on the application, sources can either be located within each time window (e.g. transient impulsive sources) or from the final stacked cross-correlations (e.g. weak and persistent sources). While computing correlations using a long window length is roughly equivalent to stacking several shorter time periods (in the absence of time-domain normalization and spectral whitening), there are many practical advantages to the latter. For each continuous data section the basic processing steps are the following:

- (i) pre-process recordings for each sensor;
- (ii) cross-correlate recordings for all unique sensor pairs;
- (iii) smooth the resulting CCFs;
- (iv) compute functional evaluations.

4.1 Pre-processing to isolate source contributions

Pre-processing of the data includes splitting data into time-windowed segments, tapering the edges, spectral whitening and bandpass filtering. In cases where multiple sources overlap in time, the resulting output power will be a superposition of probabilities which leads to ambiguity in the final locations. Effectively isolating

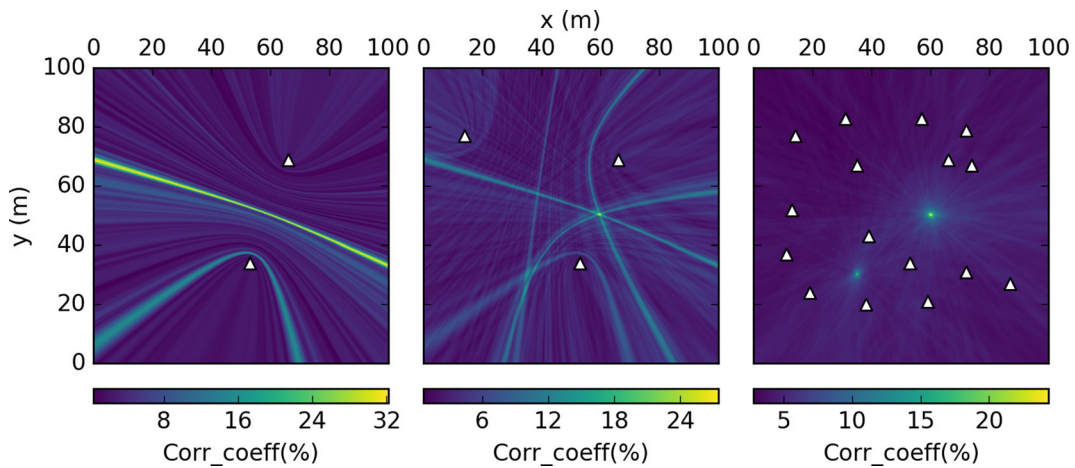


Figure 3. Effect of mapping out the cross-correlations of the synthetic seismograms in space and summing the resulting output power for 2 (left), 3 (middle) and 16 (right) sensors. Note the peaks in output power at the true source locations.

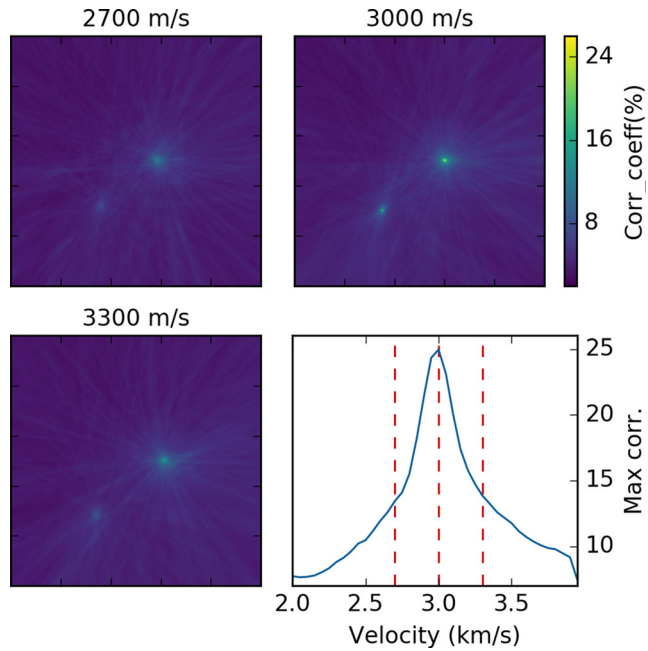


Figure 4. The effect of the chosen velocity model on the output power for the synthetic data set. Bottom right panel shows how the maximum correlation value (for the middle source) varies depending on the velocity model used to compute traveltime differences. The peak at 3000 m s^{-1} corresponds to the true velocity model used to create the simulation. This behaviour can be used to estimate and improve velocity models. Grid dimensions are the same as in Figs 2 and 3.

a single source type, by maximizing its spatial coherence across the sensor array relative to other sources, can help to reduce this ambiguity. Important parameters to consider when trying to isolate the contribution of the source of interest to the CCFs are: (1) the window length used to compute the cross-correlations, (2) time-domain normalization, and (3) frequency filtering. Settings for these parameters depend on source characteristics and the purpose of monitoring.

Determining the optimal window length involves achieving a sufficient level of spatial coherence while also limiting temporal and spatial decorrelation. Temporal decorrelation refers to non-stationarity of the source-time function (e.g. feeding of rock to ore-crusher stops) and acts to reduce power at the true source

location. Spatial decorrelation on the other hand refers to the source changing its location (e.g. moving vehicle) within the time window and leads to smearing of the focal volume and reduced output power. Equivalently, a rapidly changing medium could also be responsible for both types of decorrelation.

For the straightforward case of isolating a single impulsive source, coherence is maximized by choosing a window length equal to the duration of the source of interest plus an additional travel time allowance (determined by maximum source-sensor spacing) to ensure the arrival waveform is not clipped at the furthest sensors. This effect can be seen in the middle panel of Fig. 5 where using a narrower time window (15 ms) centred on the microearthquake significantly increases its relative output power. When trying to isolate a persistent source on the other hand, the window length needs to be long enough to achieve a sufficient level of coherence compared to the other sources present. This effect can be seen in the greater relative contribution from the persistent source (compared to the microearthquake) using the original window length (Fig. 5, left panel). As long as the persistent source remains in the same location (hence no spatial decorrelation) the upper limit on the window length will be determined by temporal decorrelation due to changes in the source-time function (i.e. the persistent source stops).

One-bit time domain normalization (see Bensen *et al.* 2007) proves beneficial for enhancing the contribution from persistent sources (e.g. crusher) that have low amplitudes relative to other possible sources (e.g. microearthquakes). As seen in the right panel of Fig. 5, although the phase of the microearthquake still correlates coherently, its contribution becomes negligible since it only occupies a small fraction of the total window length. For a more detailed discussion on the effect of time-domain normalization see Chen *et al.* (2016).

Spectral whitening is typically only beneficial when the source of interest is buried by uncorrelated noise as equalization of the spectral amplitudes will enhance its relative contribution (see Groos *et al.* 2012). Although the sources we are interested in monitoring are typically more energetic than the background wavefield (see Sections 5 and 6), we use spectral whitening in all cases for the robustness it provides through reducing the effect of strong contaminant frequencies (e.g. 50 Hz electrical noise and harmonics) commonly encountered in mine seismic systems.

Finally, the frequency range should be chosen to maximize the spatial coherence of the source of interest across the sensor array relative to other potential sources. Although not shown in the synthetic

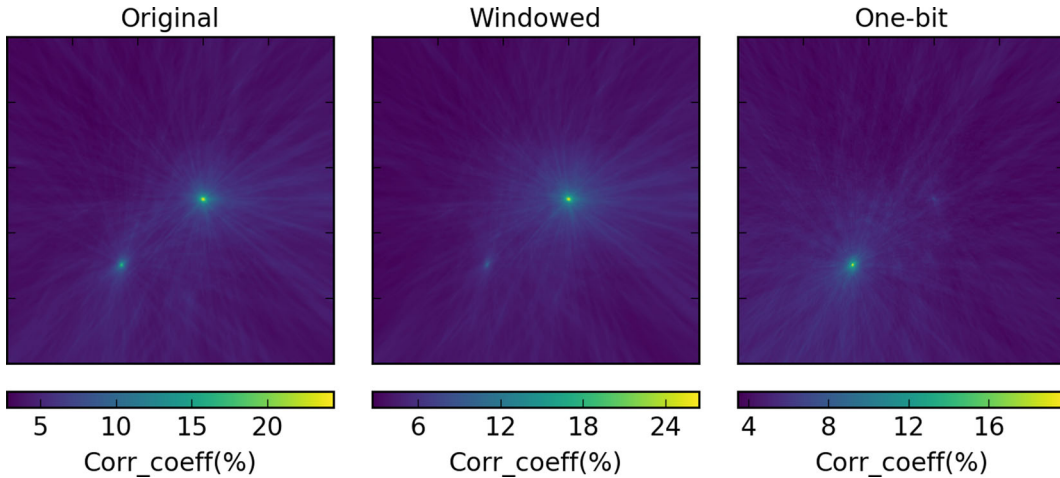


Figure 5. The effect of cross-correlation window length and one-bit time domain normalization on the relative output power of the two sources. Left: window length of 40 ms and no time-domain normalization. Middle: window length of 15 ms centred around source 1 (microearthquake) and no time-domain normalization. Right: window length of 40 ms with one-bit normalization of the original recordings. Grid dimensions are the same as in Figs 2–4.

example, this would involve choosing a higher and lower bandpass cent re frequency to isolate the microearthquake and crusher respectively.

4.2 CCF smoothing to account for uncertainties in the medium

Localization performance depends on the complexity of the medium and how accurately it can be modelled. The simplest model uses a constant velocity which allows for traveltimes to be computed analytically from the source-sensor distances assuming straight-ray propagation. The use of a constant velocity model typically requires that the signal wavelength be much greater than the length scale of heterogeneity such that they are effectively ignored. When this is not the case, it can be advantageous to use a heterogeneous velocity model and an associated wave-propagator (e.g. ray-tracing).

With our eventual goal being to perform real-time monitoring at mining sites, where computer resources are typically limited, the low computational costs associated with a homogeneous velocity model make it our method of choice. Although this has potential to greatly limit spatial resolution, we are more concerned with the general temporal and spatial patterns of seismicity as opposed to precise locations for individual microearthquakes. For this application we found the homogeneous velocity model to be a suitable choice.

If the medium has been accurately estimated (i.e. traveltimes can be accurately calculated), it is possible to beamform using the raw cross-correlated waveforms, which is referred to as coherent time-delay beamforming in matched field processing. In cases where the media has not been accurately estimated it becomes necessary to use an absolute-value smoothing process on the cross-correlated waveforms before localization. This is referred to as incoherent beamforming and ensures that coherent peaks overlap correctly in space and do not destructively interfere (due to incorrect phase shifts caused by error in the estimated velocity model).

To account for the significant error introduced by our choice of a homogeneous velocity model, we found it necessary to smooth each cross-correlation prior to computing the functional evaluations. Smoothing can be accomplished in several ways, including taking

the envelope computed from the analytic signal or, our method of choice, a sliding window root-mean-square (RMS) according to

$$\text{RMS}(t) = \sqrt{\frac{1}{N} \sum_{i=-N/2}^{N/2} x^2(t+i)} \quad (5)$$

where $x(t)$ is the signal and N is the length of the smoothing window. The appropriate setting for N depends on the uncertainty in the velocity model through the potential error in traveltime difference for two rays travelling from the same source to two separate sensors. To ensure coherent peaks correctly overlap we suggest using a smoothing window length equal to the maximum possible error in traveltime difference. The length of the smoothing window, which reflects the uncertainty in the velocity model, sets the upper bound on location accuracy and precision.

In general, sensor spacing and array aperture are also important in determining the effectiveness of beamforming techniques. For regularly spaced arrays, resolution is dictated by the minimum inter-sensor spacing through the maximum resolvable frequency (minimum of two samples per wavelength) with aliasing problems becoming an issue when inter-sensor spacing is greater than a few wavelengths. In the case of irregularly spaced arrays, however, it is no longer appropriate to use these wavelength bound limits as a minimum of two samples per wavelength is not guaranteed over the entire array (Rugrok *et al.* 2017). We did not encounter any strong aliasing effects using this specific beamforming method and refer the reader to Wathen *et al.* (2008) and (Rugrok *et al.* 2017) for more information on array responses.

4.3 Multiple wave types

Another challenge of the InterLoc method is the difficulty in accounting for multiple body wave types propagating at different velocities. For example when cross-correlating waveforms of a microearthquake with P and S arrivals recorded at two stations A and B , the resulting CCF will have physically meaningful peaks corresponding to $P_A \times P_B$ and $S_A \times S_B$ as well as spurious cross-terms $S_A \times P_B$ and $P_A \times S_B$. In the case of cross-correlating a microearthquake recorded at randomly oriented sensors, the largest amplitude peak in each CCF will most likely correspond to the correlation of the dominant energy phase, which in our case is the direct

shear-wave correlation $S_A \times S_B$. Therefore, when locating a source with CCFs containing a mix of contributions from correlating multiple phase arrivals, using the velocity of the phase with dominant amplitude should prove the most effective approach. Alternatively, isolating the P and S arrivals could be accomplished by rotating tri-axial sensors towards each potential source location.

4.4 Localization and triggering

While this technique is well suited to locate sources through an exhaustive grid search (computing a functional evaluation at every potential source location), the computational costs are steep for large search volumes. The requirement to obtain locations in near real-time for certain acoustic applications (e.g. video conferencing) has led to the development of an application specific search optimization method called stochastic region contraction (SRC; Berger & Silverman 1991; Do *et al.* 2007). In summary, given an initial search volume V_0 , this method computes the functional evaluation at J random points within the volume and then contracts the volume V_1 to enclose only the N highest values. This process continues iteratively until either a lower limit on the volume is reached, or the highest FE computed within each successive volume stabilizes, indicating that a maximum has been found. This technique has also been extended to multiple simultaneous sources by clustering the initial FEs into high probability regions containing local peaks and then using SRC on each separate region (Do & Silverman 2010). The number of functional evaluations to compute at each iteration depends on the ratio of the maximum likelihood volume V_{peak} compared to the entire search volume V_0 and the willingness to trade improved performance in exchange for lowering the probability of missing the maximum.

Running the SRC to completion during periods where sources of interest are not active is computationally wasteful. To mitigate this, we perform the following steps: after the first iteration, we compute a trigger value $T = P_{\max} - P_{\min}$ which is the difference between the maximum and minimum FE values; if T is below a predetermined threshold, then there is likely no maxima (or source) to be located and we exit the routine; trigger values that are above the threshold are considered positive triggers and the SRC procedure continues until completion. Practical application of SRC will be seen in Section 6.1.

5 CASE STUDY I: STOPING MINE

We first validate the location method using continuous seismic data from Nickel Rim South, an active underground stoping mine in Sudbury, Canada. Mine plans and the seismic system, which consists of 28 uniaxial accelerometers and 16 triaxial geophones, can be seen in Fig. 6. The seismic wavefield at this mine is dominated by drilling, blasting and microearthquakes.

5.1 Microearthquake localization

To demonstrate the effectiveness of this method in locating impulsive sources, we look first at a microearthquake of local magnitude -1.5 recorded at 27 nearby channels (mix of uni- and triaxial stations). A window length of 200 ms is used and the raw arrival signals are bandpassed from 20 to 1000 Hz and spectrally whitened (Fig. 7, left panel). From the pre-processed signals, we compute 344 CCFs (all inter-station channel pairs) and apply a sliding window RMS of length 2.2 ms. We then compute a total of 125 million functional

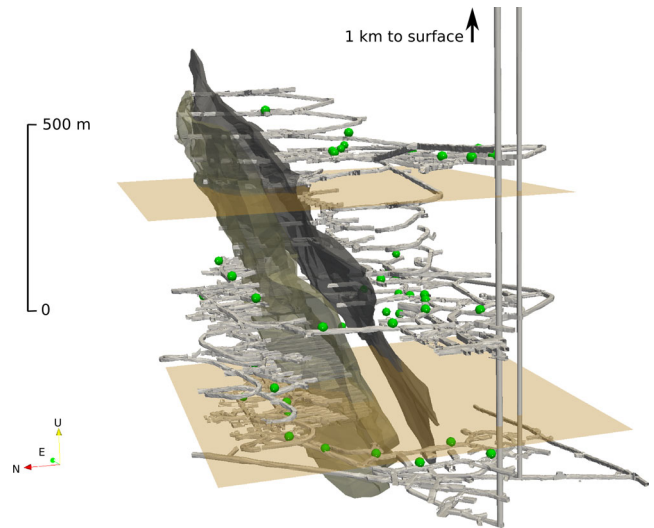


Figure 6. Mine plans for Nickel Rim South showing tunnels (light grey), ore bodies (dark grey) and sensors (green spheres). The top and bottom planes (both 500×500 m) show where the slices for the drilling and microseismic results are taken respectively.

evaluations corresponding to 1 m spacing in a 500 m^3 volume. To show the constraint on the focal volume, we plot a slice of the 3-D output power through the z -axis at the location of the global maximum in Fig. 7 (right panel). Next, we one-bit normalize the arrival waveforms and recompute the output power (Fig. 8). Although the correlation is much weaker, the event location is still clearly identifiable due to the phase coherency of the arrival waveform, which persists through amplitude normalization. Coherency of the phase allows for detection of very weak events which is not possible with traditional phase picking schemes. This will be explored further in Section 6.

5.2 Drilling localization

To demonstrate the effectiveness of this method in locating continuous sources, we use a one second period of drilling recorded at 13 nearby channels. The raw arrival signals are bandpass filtered between 500 and 2500 Hz and spectrally whitened to accentuate the drilling (Fig. 9). The ‘smearing’ effect of the maximum likelihood volume (or area for 2-D slice) is indicative of poor constraint due to lack of sensors behind the ore body at this level. Sensors from lower levels are not used in this case as they provide no additional constraint on source location. This is due to the high frequency nature of the seismic energy generated by the drilling which becomes heavily scattered and attenuated by tunnels along the ore body. Nevertheless, using only 13 sensors the InterLoc method successfully identifies and roughly localizes the non-impulsive source of seismic signal in a heavily scattering environment.

6 CASE STUDY II: BLOCK CAVING MINE

Block caving involves undercutting an ore body and allowing it to progressively collapse under its own weight and is an economical way to mine large volumes of low-grade ore. During this progressive collapse, tracking the cavefront is primarily accomplished by monitoring the location and rate of seismicity, as microearthquakes concentrate in the highly stressed rock immediately

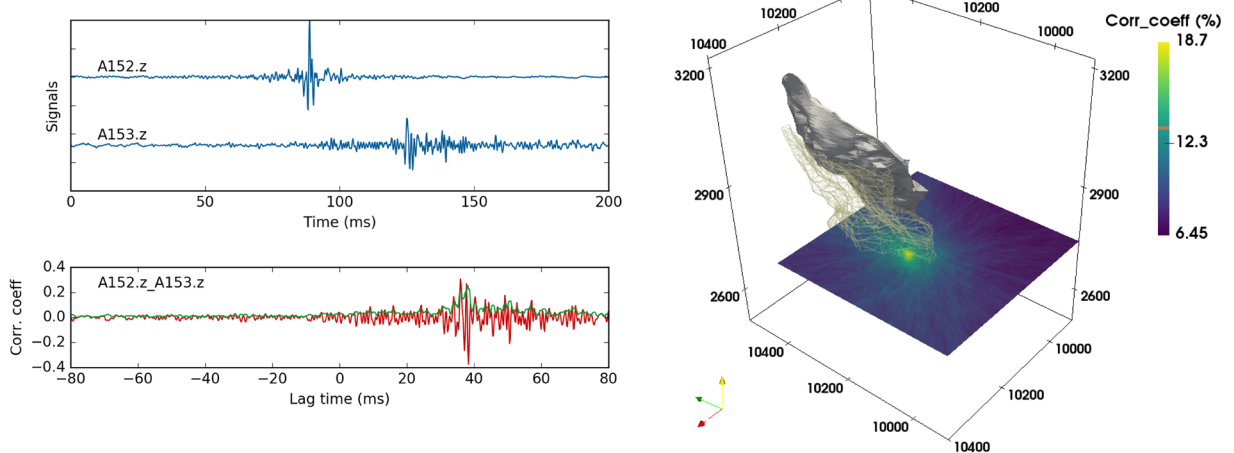


Figure 7. Left: example of seismograms for a microearthquake recorded at two sensors (top) and their resulting cross-correlation (bottom). Green solid line in bottom plot is the smoothed signal used in computing the output power. Right: slice through location of the maximum value of the summed 3-D output power computed from 344 CCFs of this event. Although not shown, constraint on focal volume is equal in all directions. Colours represent mean correlation strength in per cent.

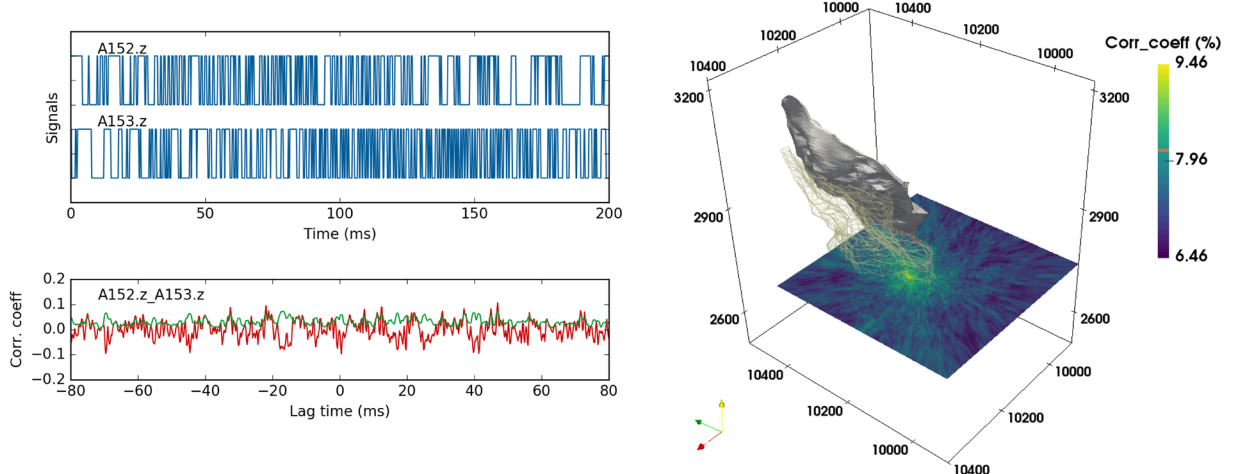


Figure 8. Same as Fig. 7 but with waveforms one-bit normalized prior to cross-correlation. Although no obvious correlation peak is discernible for this pair, the result of mapping and summing 344 CCFs still allows for localization of the microearthquake. This is possible due to the phase coherency of the event which persists through amplitude normalization.

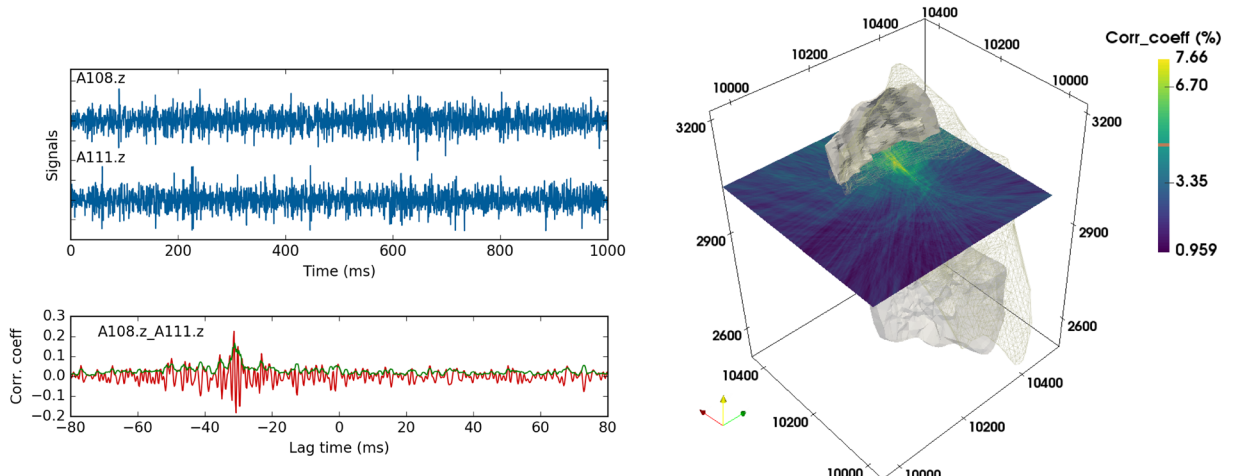


Figure 9. Same as Figs 7 and 8 but for a 1 s period of active drilling. The smearing of the maximum likelihood volume is caused by poor constraint due to lack of sensors behind the ore body at this level.

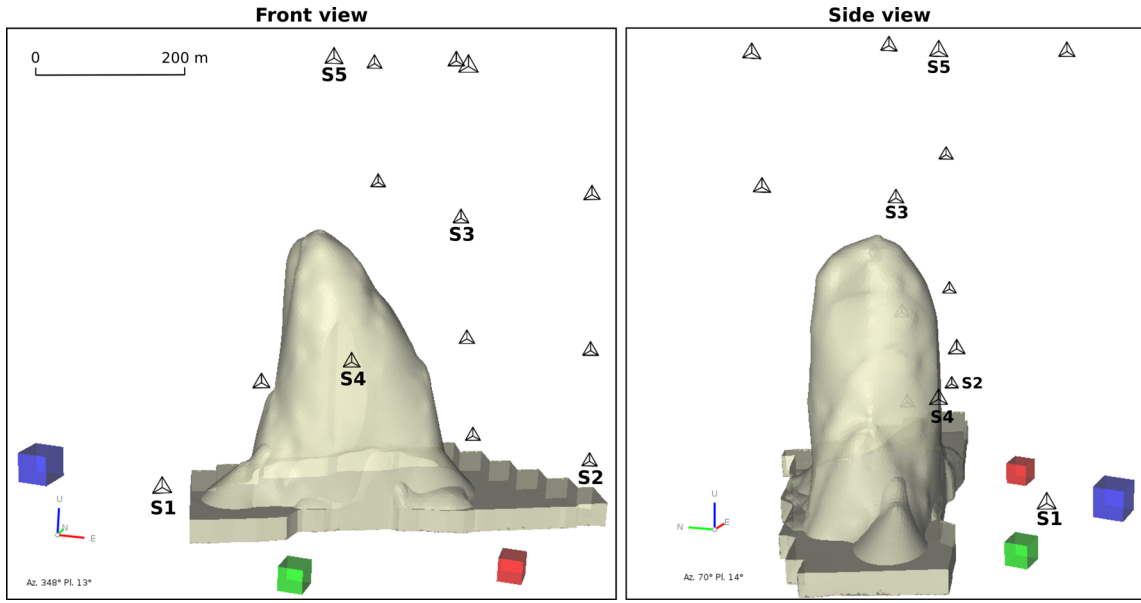


Figure 10. Mine plans for a block caving mine showing estimated cave shape in beige and ore crushers as blue, green and red respectively. Geophones shown as black triangles with labels on those specifically referred to in the text.

above the cavefront fracture zone (Mercier *et al.* 2015). Monitoring is important to ensure that the cave continues to advance and is not drifting away from the ore-body. There are also safety implications for identifying periods when the cave has stopped advancing, as continuing to extract material widens the air gap between the cavefront and the yielded material. This creates the potential for powerful and deadly air blasts if a large volume of rock yields at once, effectively jettisoning the air into the connecting tunnels.

This operation (Fig. 10) consists of an actively propagating block cave from which yielded ore is being removed and crushed. The seismic wavefield at this mine is dominated by three nearly continuously operating ore-crushers and hundreds of microearthquakes per day. The seismic system at this mine consists of over 60 triaxial geophones, however we only use a subset of data from sensors around the cave.

6.1 Microearthquake triggering

Here we evaluate the effectiveness of InterLoc in detecting and locating a full day of microearthquakes occurring around the active block cave compared to the traditional STA/LTA trigger and phase-picking scheme used at the mine. Pre-processing parameters include a cross-correlation window length of 500 ms, no time domain normalization, and a bandpass filter with corner frequencies of 200 and 1500 Hz. Time windows are overlapped by 20 per cent to ensure arrivals that span two windows are not missed. Gaps in the continuous recordings at individual sensors due to signal dropout are treated as zeros. To detect and locate microearthquakes within each 500 millisecond window, we use the SRC procedure with an initial volume of 600 m^3 , centered near the top of the cave. Within each contraction volume $J = 20\,000$ FEs are computed, sorted, and the next volume is defined around the best $N = 50$. This process is repeated until stabilization of the highest FE value, indicating a maximum has been found. This configuration was determined to be suitable based on repeatedly locating the same microearthquake (located above cave with local

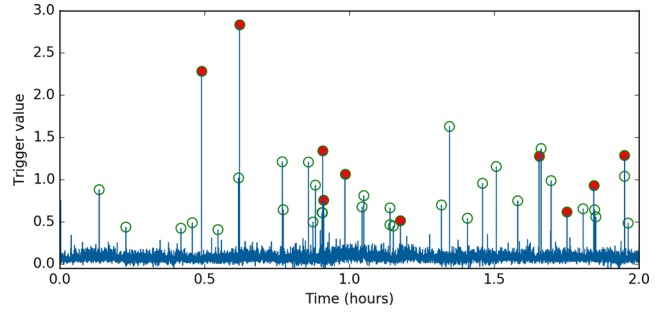


Figure 11. Plot of trigger values (see Section 4.4) over a 2 hr period a using cross-correlation window length of 500 ms with 20 per cent overlap. Values over the threshold of 0.4 (open green circles) are considered detections and subsequently located. Red filled circles indicate events that were also detected by the STA/LTA method currently being used at the mine.

magnitude -1.2) for which there is a ~ 99.7 per cent probability of finding the global maximum.

To avoid calling the SRC locator to completion during time periods with no microearthquakes we employ the triggering scheme described in Section 4.4. An example of how the trigger values vary over the first two hours of the day can be seen in Fig. 11. Using a threshold of $T = 0.4$ to signify a positive trigger we detected 585 microearthquakes, which is a great improvement compared to the 98 events (ranging in local magnitude from -2.7 to -0.2) detected by the STA/LTA triggering used at the mine. Locations for all 585 microearthquakes, as well as a comparison with the 98 events in the mine catalogue can be seen in Fig. 12. Events in the catalogue are located using a probabilistic inversion of manually picked P and S arrival times with uncertainties between 2 and 10 m. While the locations in the catalogue take advantage of the entire seismic system, those computed with InterLoc use only select sensors around the cave. This explains the larger location residuals in the poorly constrained areas further from the cave.

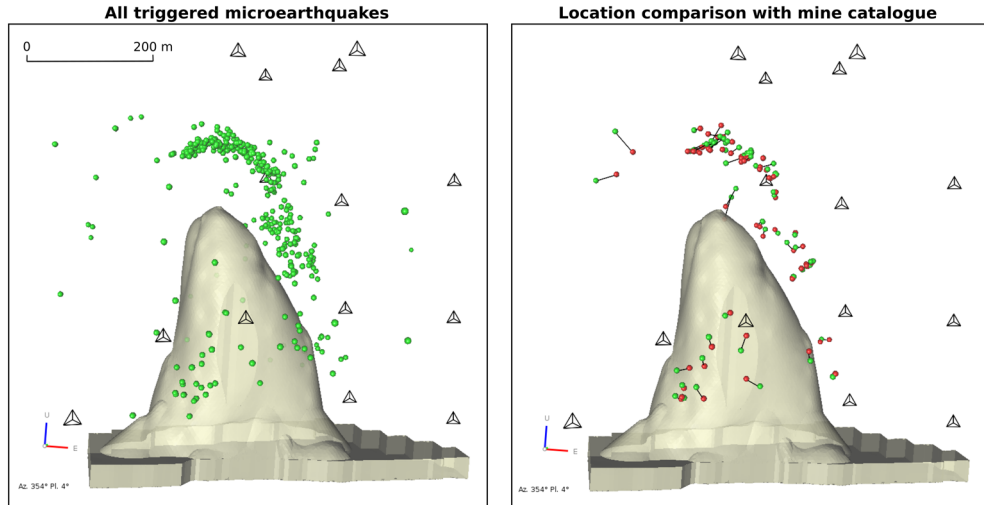


Figure 12. Left: locations for 1 d of microearthquakes as determined by InterLoc using only sensors surrounding this cave (black triangles). Note how the event distribution is concentrated in the highly stressed seismogenic zone above the cavefront which allows for inference of cave extent. Right: comparison of the location of events in the mine catalogue (red spheres) with locations of those same events as determined by InterLoc (green spheres).

6.2 Monitoring ore crusher activity

To show the potential of interferometry for temporal monitoring of persistent sources we simultaneously track the activity of all three ore-crushers at the block caving mine using a single sensor pair. Although this method does not require directly computing functional evaluations, it requires that the source locations be roughly known so that their contributions can be identified in the CCFs.

The sensor pair S1 –S2 (Fig. 10) is specifically chosen so that the crushers respective contributions to the pair's CCFs do not overlap. A cross-correlation window length of 10 s (with no overlap) is used to strike a good balance between temporal resolution and correlation strength, while bandpass corner frequencies of 40 and 400 Hz help to isolate contributions from the crushers. One-bit normalization is also used to suppress any impulsive contaminating sources such as microearthquakes. CCFs are computed for a 35 min time period (Fig. 13, middle panel) and then stacked (top panel). Since the crusher locations are known, we can identify lag time windows where each respective $S \times S$ contribution in the CCF should appear (effectively the reverse of InterLoc). The windowed signals of the stack, which represent the characteristic waveforms associated with the crushers, are used as the templates (or filters) in a template matching (or matched filter) approach. This method involves correlating the templates with their respective portions of each CCF in a semi-continuous fashion, results for which can be seen in Fig. 13 (right panel). In interpreting these results we associate active crushers with high correlation values.

The activity of each crusher appears to vary on a timescale of 5–10 min, which we believe is due to the alternating nature of the feeder and the rock-breaker with the maximum energy emitted during periods of active crushing. The template matching approach allows for identification of periods when both a single crusher (30–35 min), and multiple crushers (0–9 min) are active. Monitoring crusher activity in this manner is very easy to implement and provides higher resolution and accuracy than the hourly logs of scheduled crusher activity currently maintained by the mine. Accounting for any significant temporal changes in the medium or crusher source time functions would be as simple as updating the templates.

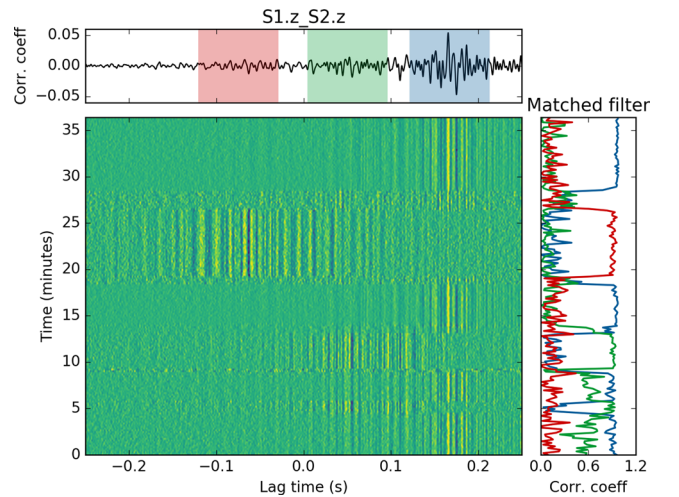


Figure 13. Individual cross-correlation functions (10 s window length) computed for a single sensor pair over a 35 min period (mid panel) and stacked (top panel). Since crusher locations are known, we build three templates (colour coded for each crusher respectively) from the stack. Right panel: the result of correlating the templates with their respective portions of each individual CCF. These values serve as a proxy for relative crusher activity at any given time.

7 POTENTIAL APPLICATION TO AMBIENT NOISE INTERFEROMETRY

In the absence of persistent sources, ambient noise interferometry can be used to estimate seismic Green's function between sensor pairs. This technique involves the cross-correlation of a spectrally white and diffuse noise field recorded at sensors A and B to estimate the Green's function G_{AB} of the sensor pair, convolved with the autocorrelation of the noise N , according to:

$$u_A(t) \otimes u_B(t) = [G_{AB}(t) + G_{AB}(-t)] * N(t). \quad (6)$$

In comparison, by cross-correlating time periods when a persistent stationary source C dominates the wavefield, we are estimating the following function:

$$u_A(t) \otimes u_B(t) = [G_{CA} * n(t)] \otimes [G_{CB} * n(t)] \quad (7)$$

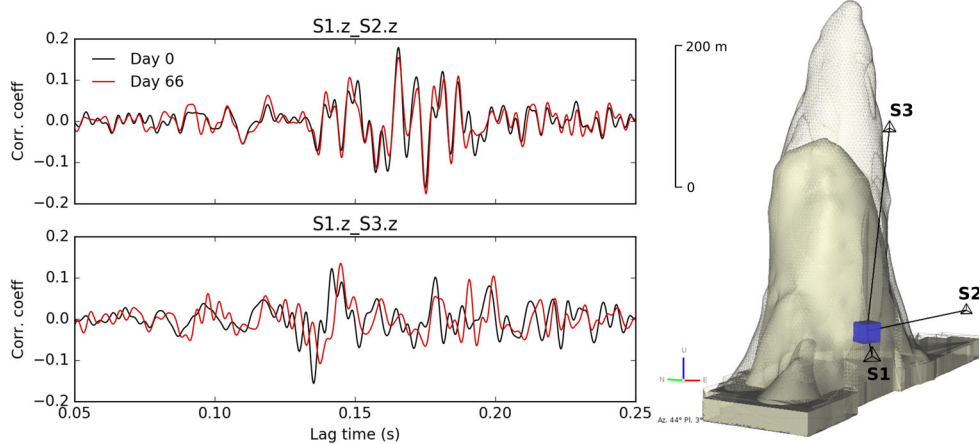


Figure 14. Cross-correlation functions for two sensor pairs computed 66 days apart, during which the block cave has propagated upwards (faded beige). Each CCF is computed from 1 min of data during which the blue crusher is dominant. The CCF in the top panel is used as the control to show that there is no change along the ray path connecting the crusher and sensor S2. The CCF in the bottom panel has shifted and changed qualitatively at certain lag-times due to changes in the medium along the ray path connecting the crusher and sensor S3. In this case the propagating block cave has delayed the maximum amplitude arrival by about 2 ms.

where $n(t)$ is the source time function of the persistent source. This can be described as the cross-correlation of the two source-sensor Green's functions convolved with the source time function of the persistent source. Although both functions (eqs 6 and 7) contain information on the medium, they are qualitatively different and must therefore be measured differently. By blindly cross-correlating and stacking data when persistent sources often dominate the wavefield, we are effectively combining these qualitatively different functions and then incorrectly interpreting the final result as the estimated Green's function for the sensor pair (eq. 6). For a correct interpretation, both the locations and nature of seismic sources need to be known so that their contributions to the final correlation function can be identified and understood as in Section 6.2.

Alternatively, instead of blindly summing all cross-correlations, we can use InterLoc to assess wavefield conditions at each time period and only stack correlations of relatively diffuse periods for a closer estimate of eq. (6). This involves evaluating the orientation of each sensor pair with respect to the energy distribution of the seismic wavefield for short successive time periods, and only time periods that are favourable are used to construct the CCFs. In this case, we identify favourable conditions as when either: (1) no strong sources are present and the wavefield is relatively diffuse; or (2) for a given sensor pair, strong sources are located in, or scattered off stationary phase locations (the conical areas behind each sensor pointing toward the other, see Roux & Kuperman 2004).

Although not shown here, we found that this form of selective stacking produces very similar results to the selective method based on the signal-to-noise ratio used by Olivier *et al.* (2015) but without the need to define an expected arrival time window and risk artificially constraining the signal. While both of these selective stacking methods are effective, they require that sufficient suitable periods exist to allow for convergence to the estimated Green's function in a reasonable amount of time. In environments where at least one strong source is always active, as with the ore-crushers at the caving mine, these periods will be very rare for the majority of sensor pairs. Moreover, selective stacking in this case appears counter-intuitive in the sense that we are trying to remove stable sources (crushers) to create stable sources (from sensors) through ambient noise interferometry.

8 TEMPORAL MONITORING WITH STABLE SOURCE INTERFEROMETRY

In this section we demonstrate how stable persistent sources, seen as contaminants in both microearthquake and ambient noise monitoring, can be used to monitor changes in the rockmass with high temporal resolution. This method follows from Section 6.2 and takes advantage of the stable waveforms created by cross-correlating time periods where one or more crushers are active. To illustrate this concept we show the potential of using the ore-crushers to monitor an advancing block cave.

As seen in the last section, by cross-correlating and stacking time periods where a single ore crusher C dominates the wavefield, we are effectively estimating eq. (7). In the situation where G_{CA} and $s_C(t)$ remain stable, changes in $u_A(t) \otimes u_B(t)$ can be attributed to changes in G_{CB} . Ignoring scattering and reflections, this Green's function is primarily determined by the direct arrivals, which are a coupling between the geometry of the least-time ray path (between C and B) and the medium along this path (described by a sensitivity kernel). Therefore, if this ray path passes through or near areas of where we expect changes in the medium, we can monitor these changes through $u_A(t) \otimes u_B(t)$.

To demonstrate this concept we compare CCFs computed 66 days apart, a period during which the block cave is estimated to have propagated upwards by ~ 180 m (Fig. 14, right panel). To show the potential temporal resolution that can be achieved, we use only 1 min of data from each day (during which the blue crusher is active) to compute the cross-correlations. CCFs were computed for two different sensor pairs: (1) $u_{S1} \otimes u_{S2}$ which is used as a control; and (2) $u_{S1} \otimes u_{S3}$, from which we hope to monitor changes. The control function is used to show that $G_{C,S1}$ remains relatively stable and therefore any changes in $u_{S1} \otimes u_{S3}$ are caused by changes in $G_{C,S3}$. We are specifically interested in changes along the ray path that connects the blue crusher with sensor S3 and passes very close to the propagating cavefront.

Results for this temporal comparison of CCF waveforms can be seen in Fig. 14 with the control pair (top panel) remaining nearly identical over the two-month period. On the other hand, comparing the $u_{S1} \otimes u_{S3}$ waveforms (bottom panel) we can see both qualitative differences as well as a time-shift of ~ 2.2 ms. We interpret the time-shift, measured by cross-correlating the two waveforms and

using the lag-time corresponding to the maximum amplitude peak, as the additional traveltimes incurred by the direct S-wave having to now partially circumvent the cave. This additional traveltimes is equivalent to ~ 7 m of additional propagation distance at a velocity of 3200 m s $^{-1}$, which agrees with the changes in cave geometry with respect to this ray path.

The main advantage of this technique over ambient noise interferometry is the high temporal resolution afforded by strong sources, as opposed to relying on the weak multiply scattered seismic wavefield. Future work will involve monitoring these waveforms (computed for multiple sensor pairs) in semi-continuous time, to improve spatio temporal constraint on the propagating cave. Hopefully this method will be considered when designing mine seismic systems by ensuring some crusher-sensor ray paths sample areas of interest.

9 CONCLUSIONS

Detection and location of seismic sources is still predominantly accomplished using triggering and phase-picking methods. Originally developed with the impulsive nature of earthquake rupture in mind, these methods fail under conditions when arrival times cannot be accurately picked; typically when sources are weak, persistent or simultaneously active. The interference of arrival waveforms, accomplished through cross-correlation, provides a robust alternative by removing the need to identify arrival phases. This is a key component in the interferometric locator, a proven and popular localization method which utilizes spectrally whitened cross-correlations in a beamforming-like approach. The success of this technique lies in the robustness of cross-correlations, the insensitivity to environmental conditions exhibited by spectral whitening, and the localization advantages of a steered beamformer. Practical considerations for this technique include pre-processing of the signals to isolate sources of interest, calculating traveltimes based on the velocity of the dominant amplitude phase and smoothing of the CCFs prior to localization to account for uncertainties in the medium. While an exhaustive grid-search for potential source locations is possible, we recommend implementing the SRC procedure for its computational efficiency and simple parametrization.

The robustness of the InterLoc method was demonstrated through the detection, location and monitoring of a variety of seismic sources with three different data sets. The synthetic data set showed the ability of the method in locating two simultaneous sources under different processing parameters, while data from two active underground mines was used to effectively monitor both impulsive and persistent sources. While InterLoc maps CCFs into space, there is also value in the reverse process which is mapping a known source location to its respective lag-time in a CCF. Using this method, we were able to simultaneously monitor the activity of all three ore-crushers at a block caving mine using cross-correlations from a single sensor pair in a template matching approach. Information on source locations and activity can also be integrated with ambient noise interferometry to improve estimates of seismic Green's functions under temporally variable and anisotropic wavefield conditions. This involves creating a selective stacking filter that evaluates the orientation of each sensor pair with respect to the energy distribution of the seismic wavefield for short successive time periods, and only time periods that are favourable are used to estimate the final Green's functions. Additionally, we demonstrated how CCFs of strong persistent sources (ore-crushers), typically seen as contaminants in both microearthquake and ambient noise monitoring, can be used to monitor changes in the medium between source and sensors. The main advantage of this technique over ambient noise

interferometry is the high temporal resolution afforded by strong sources, as opposed to relying on the weak multiply scattered field.

ACKNOWLEDGEMENTS

Thanks to IMS research patrons (A-CFT) for supporting this research, Michael Afanasiev for helping with the simulations and Brad Simser at Nickel Rim South. We also acknowledge the two anonymous reviewers for their insightful comments that helped improve this paper. This work was funded by Natural Science and Engineering Research Council of Canada through Discovery Grant #418288-2012 and Engage Grant #EGP 469949-14 to PA.

REFERENCES

- Afanasiev, M., Boehm, C., van Driel, M., Krischer, L., May, D.A., Rietmann, M. & Fichtner, A., 2017. Salvus: An open-source high-performance package for full waveform modelling and inversion from laboratory to global scales, note: 0.0.1-475-gc87fc6d1, doi:10.5905/ethz-1007-88.
- Allen, R.V., 1978. Automatic earthquake recognition and timing from single traces, *Bull. seism. Soc. Am.*, **68**(5), 1521–1532.
- Allen, R.M. & Kanamori, H., 2003. The potential for earthquake early warning in southern California, *Science*, **300**(5620), 786–789.
- Ballmer, S., Wolfe, C.J., Okubo, P.G., Haney, M.M. & Thurber, C.H., 2013. Ambient seismic noise interferometry in Hawai'i reveals long-range observability of volcanic tremor, *Geophys. J. Int.*, **194**(1), 512–523.
- Bensen, G.D., Ritzwoller, M.H., Barmin, M.P., Levshin, A.L., Lin, F., Moschetti, M.P., Shapiro, N.M. & Yang, Y., 2007. Processing seismic ambient noise data to obtain reliable broad-band surface wave dispersion measurements, *Geophys. J. Int.*, **169**(3), 1239–1260.
- Berger, M.F. & Silverman, H.F., 1991. Microphone array optimization by stochastic region contraction, *IEEE Trans. Signal Process.*, **39**(11), 2377–2386.
- Brenguier, F., Shapiro, N.M., Campillo, M., Ferrazzini, V., Duputel, Z., Coutant, O. & Nercissian, A., 2008. Towards forecasting volcanic eruptions using seismic noise, *Nat. Geosci.*, **1**(2), 126–130.
- Bucker, H.P., 1976. Use of calculated sound fields and matched-field detection to locate sound sources in shallow water, *J. acoust. Soc. Am.*, **59**(2), 368–373.
- Campillo, M., 2006. Phase and correlation in ‘random’ seismic fields and the reconstruction of the Green function, *Pure appl. Geophys.*, **163**(2), 475–502.
- Chen, Z., Gerstoft, P. & Bromirski, P.D., 2016. Microseism source direction from noise cross-correlation, *Geophys. J. Int.*, **205**(2), 810–818.
- Claerbout, J.F., 1968. Synthesis of a layered medium from its acoustic transmission response, *Geophysics*, **33**(2), 264–269.
- Corciulo, M., Roux, P., Campillo, M., Dubucq, D. & Kuperman, W.A., 2012. Multiscale matched-field processing for noise-source localization in exploration geophysics, *Geophysics*, **77**(5), KS33–KS41.
- Cros, E., Roux, P., Vandemeulebrouck, J. & Kedar, S., 2011. Locating hydrothermal acoustic sources at old faithful geyser using matched field processing, *Geophys. J. Int.*, **187**(1), 385–393.
- DiBiase, J., 2000. A High-Accuracy, Low-Latency Technique for Talker Localization in Reverberant Environments Using Microphone Arrays, *PhD thesis*, Brown University.
- DiBiase, J.H., Silverman, H.F. & Brandstein, M.S., 2001. *Robust Localization in Reverberant Rooms*, pp. 157–180, Springer.
- Do, H. & Silverman, H.F., 2010. SRP-PHAT methods of locating simultaneous multiple talkers using a frame of microphone array data, in *2010 IEEE International Conference on Acoustics, Speech and Signal Processing*, Honolulu, Hawaii, pp. 125–128.
- Do, H., Silverman, H.F. & Yu, Y., 2007. A real-time SRP-PHAT source location implementation using stochastic region contraction (SRC) on a large-aperture microphone array, in *2007 IEEE International Conference on Acoustics, Speech and Signal Processing - ICASSP '07*, Dallas, Texas, Vol. 1, pp. I-121–I-124.

- Droznin, D., Shapiro, N., Droznina, S.Y., Senyukov, S., Chebrov, V. & Gordeev, E., 2015. Detecting and locating volcanic tremors on the Klyuchevskoy group of volcanoes (Kamchatka) based on correlations of continuous seismic records, *Geophys. J. Int.*, **203**(2), 1001–1010.
- Geiger, L., 1912. Probability method for the determination of earthquake epicenters from the arrival time only, *Bull. St. Louis Univ.*, **8**, 60–71.
- Groos, J., Bussat, S. & Ritter, J., 2012. Performance of different processing schemes in seismic noise cross-correlations, *Geophys. J. Int.*, **188**(2), 498–512.
- Hahn, W. & Tretter, S., 1973. Optimum processing for delay-vector estimation in passive signal arrays, *IEEE Trans. Inf. Theory*, **19**(5), 608–614.
- Kao, H. & Shan, S.-J., 2004. The source-scanning algorithm: mapping the distribution of seismic sources in time and space, *Geophys. J. Int.*, **157**(2), 589–594.
- Knapp, C. & Carter, G., 1976. The generalized correlation method for estimation of time delay, *IEEE Trans. Acoust. Speech Signal Process.*, **24**(4), 320–327.
- Kuperman, W. & Turek, G., 1997. Matched field acoustics, *Mech. Syst. Signal Process.*, **11**(1), 141–148.
- Lobkis, O.I. & Weaver, R.L., 2001. On the emergence of the Green's function in the correlations of a diffuse field, *J. acoust. Soc. Am.*, **110**(6), 3011–3017.
- Marchand, N., 1964. Error distributions of best estimate of position from multiple time difference hyperbolic networks, *IEEE Trans. Aerosp. Navigational Electron.*, **ANE-11**(2), 96–100.
- Mercier, J.-P., de Beer, W., Mercier, J.-P. & Morris, S., 2015. Evolution of a block cave from time-lapse passive source body-wave traveltimes tomography, *Geophysics*, **80**(2), WA85–WA97.
- Obara, K., 2002. Nonvolcanic deep tremor associated with subduction in southwest Japan, *Science*, **296**(5573), 1679–1681.
- Olivier, G., Brenguier, F., Campillo, M., Lynch, R. & Roux, P., 2015. Body-wave reconstruction from ambient seismic noise correlations in an underground mine, *Geophysics*, **80**(3), KS11–KS25.
- Roux, P. & Kuperman, W.A., 2004. Extracting coherent wave fronts from acoustic ambient noise in the ocean, *J. acoust. Soc. Am.*, **116**(4), 1995–2003.
- Ruigrok, E., Gibbons, S. & Wapenaar, K., 2017. Cross-correlation beam-forming, *J. Seismol.*, **21**(3), 495–508.
- Sabra, K.G., Roux, P. & Kuperman, W.A., 2005. Emergence rate of the time-domain Green's function from the ambient noise cross-correlation function, *J. acoust. Soc. Am.*, **118**(6), 3524–3531.
- Sens-Schönfelder, C. & Wegler, U., 2006. Passive image interferometry and seasonal variations of seismic velocities at Merapi volcano, Indonesia, *Geophys. Res. Lett.*, **33**, L21302, doi:10.1029/2006GL027797.
- Shapiro, N.M. & Campillo, M., 2004. Emergence of broadband Rayleigh waves from correlations of the ambient seismic noise, *Geophys. Res. Lett.*, **31**, L07614, doi:10.1029/2004GL019491.
- Shapiro, N.M., Ritzwoller, M.H. & Bensen, G.D., 2006. Source location of the 26 sec microseism from cross-correlations of ambient seismic noise, *Geophys. Res. Lett.*, **33**, L18310, doi:10.1029/2006GL027010.
- Snieder, R., 2004. Extracting the Green's function from the correlation of coda waves: a derivation based on stationary phase, *Phys. Rev. E*, **69**, 046610, doi:10.1103/PhysRevE.69.046610.
- Wassermann, J., 1997. Locating the sources of volcanic explosions and volcanic tremor at Stromboli volcano (Italy) using beam-forming on diffraction hyperboloids, *Phys. Earth planet. Inter.*, **104**(1), 271–281.
- Wathelet, M., Jongmans, D., Ohrnberger, M. & Bonnefoy-Claudet, S., 2008. Array performances for ambient vibrations on a shallow structure and consequences over Vs inversion, *J. Seismol.*, **12**(1), 1–19.
- Wax, M. & Kailath, T., 1983. Optimum localization of multiple sources by passive arrays, *IEEE Trans. Acoust. Speech Signal Process.*, **31**(5), 1210–1217.
- Weaver, R.L. & Lobkis, O.I., 2004. Diffuse fields in open systems and the emergence of the Green's function (L), *J. acoust. Soc. Am.*, **116**(5), 2731–2734.